

# Isotropic Proton-detected Local-field Nuclear Magnetic Resonance in Solids

Robert H. Havlin,<sup>\*</sup> Jamie D. Walls,<sup>†</sup> and Alexander Pines<sup>‡</sup>

*Materials Sciences Division, Lawrence Berkeley National Laboratory, Berkeley, CA 94720*

*Department of Chemistry, University of California at Berkeley, Berkeley, CA 94720*

(Dated: July 24, 2004)

## Abstract

A new nuclear magnetic resonance (NMR) method is presented which produces linear, isotropic proton-detected local-field spectra for  $I_N S$  spin systems in powdered samples. The method, HETeronuclear Isotropic Evolution (HETIE), refocuses the anisotropic portion of the heteronuclear dipolar coupling frequencies by evolving the system under a series of specially designed Hamiltonians and evolution pathways. The theory behind HETIE is presented along with experimental studies conducted on a powdered sample of ferrocene, demonstrating the methodology outlined in this paper. Applications of HETIE for structural determination in solid-state NMR are discussed.

PACS numbers:

## I. INTRODUCTION

The determination of the molecular structure is central to our understanding of complex chemical systems. During the past century, structural techniques such as X-ray crystallography and more recently liquid state NMR have tremendously advanced our comprehension of molecular processes in nature. However, some systems such as the prion protein<sup>1,2</sup>, spider silk<sup>3</sup>, amyloid fibrils<sup>4</sup>, and frozen snapshots of protein folding<sup>5</sup> are not amenable to liquid state NMR structural studies or X-ray crystallographic techniques. In such systems where these otherwise robust techniques fall short, solid-state NMR has become a valuable technique. Solid-state NMR utilizes interactions such as dipole-dipole couplings and/or chemical shift anisotropy (CSA), which are present in solids and are very sensitive to molecular structure. In particular, dipole-dipole couplings, due to their dependence upon the distance between the interacting spins, have already provided useful structural constraints for molecules in solids<sup>6</sup>.

Although there have been many attempts to further develop the use of dipolar couplings for use in structure determination, the progress of these methods has been impeded by the Zeeman field-induced angular dependence of the dipolar frequencies, which hinders the extraction of the desired distance information from the spectrum. In the presence of a large Zeeman field, taken to be along the  $\hat{z}$ -axis, the heteronuclear dipolar Hamiltonian between an  $I$  and  $S$  spin is given by

$$H_D^{\text{HF}} = \omega_D \frac{3 \cos(\theta_L)^2 - 1}{2} (2I_Z S_Z) \quad (1)$$

where  $\theta_L$  is the angle that the internuclear vector  $\vec{r}_{IS}$  makes with respect to the Zeeman field. The dipolar coupling constant is given by  $\omega_D = \frac{\gamma_I \gamma_S}{|\vec{r}_{IS}|^3}$  where  $\gamma_I$  and  $\gamma_S$  are the gyromagnetic ratios of spin  $I$  and  $S$  respectively. For a powdered sample, the spectrum consists of a typical Pake pattern for a pair dipole coupled spins [Figure 1(A)] since the eigenvalues of  $H_D^{\text{HF}}$  depend upon  $\theta_L$ . This anisotropic broadening limits resolution, lowers sensitivity, and complicates spectral assignments of dipolar couplings in solids. One of the main objectives of developing a dipolar coupling based structural technique is to remove the anisotropic nature of observed couplings.

Since the anisotropy of the dipolar frequencies in a powdered sample is due to the presence of a large Zeeman field, many methods have been developed which either evolve the system in zero-field<sup>7,8</sup> or make the system appear to have evolved in zero-field through the application of

some multiple-pulse sequence<sup>9-12</sup>. The zero-field dipolar Hamiltonian is given by

$$\begin{aligned} H_D^{\text{ZF}} &= \omega_D (\vec{I} \cdot \vec{S} - 3(\vec{I} \cdot \hat{r}_{IS})(\vec{S} \cdot \hat{r}_{IS})) \\ &= \omega_D \sum_{m=-2}^2 (-1)^m A_{2,m}^{IS}(\theta_{IS}, \phi_{IS}) T_{2,-m}^{IS} \end{aligned} \quad (2)$$

where  $A_{2,m}^{IS}(\theta_{IS}, \phi_{IS})$  and  $T_{2,m}^{IS}$  are second rank spatial and spin tensors respectively, and  $(\theta_{IS}, \phi_{IS})$  are polar angles relating the spin quantization axis to  $\vec{r}_{IS}$ . The eigenvalues of  $H_D^{\text{ZF}}$  are independent of  $\theta_{IS}$  and  $\phi_{IS}$ , which, even for a powdered sample, result in three sharp peaks [Figure 1(B)].

Tycko<sup>9-11</sup> demonstrated for a homonuclear spin system that the dipolar Hamiltonian in high-field can be manipulated by a series of rotor-synchronized radiofrequency (RF) pulses such that the system appears to evolve under an effective Hamiltonian proportional to  $H_D^{\text{ZF}}$  over the duration of the pulse sequence. Although Tycko's methodology has only been demonstrated for homonuclear spin systems, it is possible to extend the method to create an isotropic zero-field Hamiltonian for the heteronuclear case.  $H_D^{\text{HF}}$  can be rewritten as follows:

$$\begin{aligned} H_D^{\text{HF}} &= \omega_D \frac{3 \cos^2(\theta_L) - 1}{2} 2I_Z S_Z \\ &= \frac{2}{3} \omega_D A_{2,0}^{IS}(\theta_L) (3I_Z S_Z - \vec{I} \cdot \vec{S} + \vec{I} \cdot \vec{S}) \\ &= \frac{2}{3} \omega_D A_{2,0}^{IS}(\theta_L) (T_{2,0}^{IS} + T_{0,0}^{IS}) \\ &= \frac{2}{3} \omega_D \left[ \sum_{l=0,2,4} C(l, 0, 2, 0, 2, 0) F_{l,0} + C(2, 0, 2, 0, 0, 0) F'_{2,0} \right] \end{aligned} \quad (3)$$

where the  $C(2, 2, l, 0)$  are Clebsch-Gordon coefficients, and  $F_{l,0}$  are spherical tensors in the combined space of spin and space. Note that  $F'_{2,0}$  and  $F_{2,0}$  describe different second rank tensors in the combined space. The scalar term,  $F_{0,0}$ , is rotationally invariant to any combined rotation of space and spin and hence is proportional to the zero-field Hamiltonian,  $H_D^{\text{ZF}}$ , in Eq. (3). If a pulse sequence is implemented which removes all the second and fourth rank tensors in the combined space of spin and space from  $H_D^{\text{HF}}$ , then the zero-field Hamiltonian is obtained with a maximum scaling factor given by  $\sigma_{\text{MAX}} = 2/15$ . The resulting spectrum obtained would consist of three sharp peaks at frequencies 0 Hz and  $\pm 3\omega_D/(20\pi)$  Hz. For an  $I_N S$  spin system, the homonuclear couplings between the I spins can in principle be removed without removing the heteronuclear interactions since the I and S spins can be independently manipulated under high-field conditions.

Even though the anisotropy has been removed leading to sharp spectral features, the spectrum under the zero-field Hamiltonian [Eq. (3)] for an  $I_N S$  system can still be quite difficult to interpret.

Consider the scenario of an  $I_2S$  system where the dipole-dipole coupling between the I spins has been removed, and, through some method, the zero-field dipolar Hamiltonian between the I and S spins has been created. The resulting zero-field Hamiltonian is given by

$$\begin{aligned}
H_D^{\text{ZF}} &= \sum_{m=-2}^2 [\omega_D^{S1} (-1)^m T_{2,m}^{S1} A_{2,-m}^{S1}(\theta_{S1}, \phi_{S1}) + \omega_D^{S2} (-1)^m T_{2,m}^{S2} A_{2,-m}^{S2}(\theta_{S2}, \phi_{S2})] \\
&= \omega_D^{S1} (3S_Z I_Z^1 - \vec{S} \cdot \vec{I}^1) + \omega_D^{S2} (3S_Z I_Z^2 - \vec{S} \cdot \vec{I}^2) \\
&= H_{D,S1}^{\text{ZF}} + H_{D,S2}^{\text{ZF}}
\end{aligned} \tag{4}$$

where a collinear geometry has been chosen for the  $I_2S$  system. The spectra corresponding to evolution of the total magnetization of the I spins,  $1/3 \sum_{j=X,Y,Z} \text{Trace}[I_j \exp(itH_D^{\text{ZF}}) I_j \exp(-itH_D^{\text{ZF}})]$  are shown in Figs. 2(A) and 2(C) for two different sets of dipolar couplings. The spectra contain features that are not simply related to the couplings. This is due to the fact that typically the zero-field couplings do not commute with one another, i.e.,  $[H_{D,S1}^{\text{ZF}}, H_{D,S2}^{\text{ZF}}] \neq 0$ . The corresponding spectra therefore contain features which are not linear in the number of spins, making interpretation difficult. This is in contrast to standard proton-detected local field (PDLF) spectroscopy as shown in Figures 2(B) and 2(D). Here the high-field Hamiltonian [Eq. (1)] was used for one crystallite orientation ( $\theta_L = 0^\circ$ ). In the absence of homonuclear dipolar couplings, the resulting spectra are linear in the number of spins, with the splitting of each doublet equal to the effective heteronuclear coupling. In most PDLF experiments, the protons are decoupled from one another and evolve under the heteronuclear coupling to another nucleus, typically a  $^{13}\text{C}$ . Most PDLF experiments have been implemented in oriented phases where nonzero, motionally averaged dipolar couplings exist. This results in N sharp doublets where the motionally averaged heteronuclear dipolar couplings can be interpreted quite readily<sup>13,14</sup>. Applications of PDLF spectra to solids have also been performed; however, the resulting spectra consist of N overlapping Pake patterns, which due to the anisotropy in Eq. (1), are difficult to interpret<sup>15,16</sup>.

Recently an alternative method was proposed, called HOMonuclear Isotropic Evolution (HOMIE), which produces isotropic dipolar spectra for pairs of homonuclear coupled spin systems<sup>17</sup>. The HOMIE method works as follows: from Eq. (1) the observed dipolar frequencies are proportional to  $\omega_D(3 \cos^2(\theta) - 1)$ . If another Hamiltonian is generated with frequencies proportional to  $\omega_D \sin^2(\theta)$ , the anisotropic contribution to the combined signal is cancelled using the relation  $\sin^2(\theta) + \cos^2(\theta) = 1$ . Unlike the ZFHF method, only the frequencies are combined

in order to remove the anisotropy. Such problems as noncommuting couplings therefore do not enter into the HOMIE methodology, and proton-detected local-field spectra, such as those shown in Figure 2(B), should be possible to obtain in powdered samples.

In the following article, the HOMIE methodology is applied to heteronuclear spin systems in order to produce isotropic dipolar spectra. The method, called HETeronuclear Isotropic Evolution (HETIE), produces isotropic proton-detected local-field spectra. For an  $I_N S$  spin system, HETIE generates  $N$  doublets with splittings proportional to the heteronuclear coupling. The basic theory for HETIE is first presented, followed by a set of multiple-pulse sequences which can be used to implement the HETIE method. Finally, the HETIE method is applied to a sample of ferrocene in order to experimentally validate the method.

## II. THEORY

The Hamiltonian for an  $I_N S$  spin system in the solid-state under sample rotation and RF radiation is given by

$$H_{\text{sys}} = H_{II}(t) + H_{IS}(t) + H_I(t) + H_S(t) + H_{RF}^I(t) + H_{RF}^S(t) \quad (5)$$

where  $H_{II}(t)$  and  $H_{IS}(t)$  are the homonuclear dipolar and heteronuclear isotropic scalar and dipolar couplings.  $H_I(t)$  and  $H_S(t)$  are the chemical shift and chemical shift anisotropy (CSA) Hamiltonians for the  $I$  and  $S$  spins respectively, and  $H_{RF}^I(t)$  and  $H_{RF}^S(t)$  are the radiofrequency (RF) Hamiltonians applied to the  $I$  and  $S$  spins respectively. The explicit forms of the various Hamiltonians are given by

$$H_{II}(t) = \sum_{i < j} \omega_D^{ij}[\theta_{ij}(t)] \left( 3I_Z^i I_Z^j - \vec{I}^i \cdot \vec{I}^j \right) \quad (6)$$

$$H_{IS}(t) = \sum_j (2\omega_D^j[\theta_{jS}(t)] + J_j) I_Z^j S_Z \quad (7)$$

$$H_{I(S)}(t) = \sum_j \Omega_j^{I(S)}[\theta_j(t), \phi_j(t)] I_Z^j(S_Z) \quad (8)$$

$$H_{RF}^{I(S)}(t) = \omega_{RF}^{I(S)}(t) [I_X(S_X) \cos(\phi^{I(S)}(t)) + I_Y(S_Y) \sin(\phi^{I(S)}(t))] \quad (9)$$

where  $\theta(t)$  and  $\phi(t)$  in Eq. (6) - Eq. (9) are the angles which relate the principal axis system (PAS) of the various interactions in  $H_{\text{sys}}$  to the laboratory frame defined by the Zeeman axis. The angles,  $\theta(t)$  and  $\phi(t)$ , are shown to be time-dependent in order to take into account the possibility

of mechanical rotation of the sample. Under mechanical rotation at a frequency  $\omega_r$  about an axis which makes an angle of  $\theta_r$  with respect to the Zeeman field, the spatial factors in  $H_{\text{sys}}$ ,  $\omega_{\text{Int}}(\theta(t), \phi(t))$ , transform as

$$\omega_{\text{Int}}(\theta(t), \phi(t)) = \sum_{m=-2}^2 d_{m,0}^2(\theta_r) \exp(-im\omega_r t) \omega_{\text{Int}}^m(\theta_{\text{rot.fr}}, \phi_{\text{rot.fr}}) \quad (10)$$

where  $d_{m,0}^2(\theta_r)$  is the reduced Wigner-rotation matrix element, and  $\omega_{\text{Int}}^m(\theta_{\text{rot.fr}}, \phi_{\text{rot.fr}})$  represents the spatial part of  $H_{\text{Int}}$  in the rotor frame. For example, the explicit form of either  $\omega_D^{ij}(\theta_{ij}(t))$  or  $\omega_D^j(\theta_{jS}(t))$  is:

$$\begin{aligned} \omega_D(\theta(t)) &= \omega_D \frac{3 \cos^2(\theta(t)) - 1}{2} \\ &= \frac{1}{4} (3 \cos^2(\theta_{\text{rot.fr}}) - 1) (3 \cos^2(\theta_r) - 1) \\ &\quad + \frac{3}{4} \sin^2(\theta_{\text{rot.fr}}) \sin^2(\theta_r) \sin(2[\omega_r t + \phi_{\text{rot.fr}}]) \\ &\quad + \frac{3}{4} \sin(2\theta_{\text{rot.fr}}) \sin(2\theta_r) \sin(\omega_r t + \phi_{\text{rot.fr}}) \end{aligned} \quad (11)$$

As can be seen from Eq. (11),  $\omega_D(\theta(t))$  will contain terms proportional both to  $\sin^2(\theta_{\text{rot.fr}})$  and  $\cos^2(\theta_{\text{rot.fr}})$ . In the following, the subscripts *rot.fr* will be dropped, and all angles,  $\theta$  and  $\phi$ , will be written in the rotor frame.

The basic ideas behind HETIE follow from the HOMIE method<sup>17</sup>. As in the HOMIE experiments, rotor-synchronized multiple-pulse sequences are used in order to create certain average Hamiltonians<sup>18,19</sup> which the system evolves under in order to obtain isotropic dipolar spectra. The necessary Hamiltonians used in HETIE are (up to an overall constant)

$$H = \sum_j \left( k\omega_D^j \frac{3 \cos^2(\theta_{jS}) - 1}{2} + \frac{J_j}{2} k' \right) I_X^j 2S_Z \quad (12)$$

$$H^{\text{EVO}} = \sum_j g\omega_D^j \sin^2(\theta_{jS}) (\exp(i2\phi_{jS}) I_+^j + \exp(-i2\phi_{jS}) I_-^j) 2S_Z \quad (13)$$

$$H_{\pm 1}^{\text{DET}} = \sum_j f\omega_D^j \sin(2\theta_{jS}) (\exp(\pm i\phi_{jS}) I_+^j + \exp(\mp i\phi_{jS}) I_-^j) 2S_Z \quad (14)$$

The pulse sequences which generate  $H$ ,  $H^{\text{EVO}}$ , and  $H_{\pm 1}^{\text{DET}}$  are given in the next section. Since the heteronuclear couplings between the  $I$  spins commute, and the homonuclear interactions between the  $I$  spins are assumed to have been removed, the evolution for each  $I$  spin can be calculated independently from one another.

Starting with  $\rho(0) = \sum_j a_j I_Z^j$ , evolution under  $H$  for a time  $t$  gives

$$\begin{aligned}
\rho(t) &= \exp(-itH)\rho(0)\exp(itH) \\
&= \sum_j a_j [I_Z^j \cos(k(\theta_{jS})t) - 2S_Z I_Y^j \sin(k(\theta_{jS})t)] \\
&= \sum_j a_j [\rho_0^j(t) + \rho_1^j(t)]
\end{aligned} \tag{15}$$

where

$$\rho_0^j = I_Z^j \cos(k(\theta_{jS})t) \tag{16}$$

$$\rho_1^j = -2S_Z I_Y^j \sin(k(\theta_{jS})t) \tag{17}$$

where  $k(\theta_{jS}) = k\omega_D^j(3\cos^2(\theta_{jS}) - 1)/2 + J_j k'/2$ . Each of the pathways,  $\rho_0$  and  $\rho_1$ , can be distinguished by their rotational property under a z-rotation, and each pathway will be considered separately, which is depicted in Figure 3. Evolution for a time  $\tau$  under  $H^{\text{EVO}}$  gives the following:

$$\begin{aligned}
\rho_0(t, \tau) &= \exp(-i\tau H^{\text{EVO}}) \rho_0(t) \exp(i\tau H^{\text{EVO}}) \\
&= \sum_j a_j I_Z^j \cos(k(\theta_{jS})t) \cos(2g(\theta_{jS})\tau) \\
&\quad - 2a_j S_Z I_Y^j \cos(k(\theta_{jS})t) \sin(2g(\theta_{jS})\tau) \cos(2\phi_{jS}) \\
&\quad - 2a_j S_Z I_X^j \cos(k(\theta_{jS})t) \sin(2g(\theta_{jS})\tau) \sin(2\phi_{jS})
\end{aligned} \tag{18}$$

$$\begin{aligned}
\rho_1(t, \tau) &= \exp(-i\tau H^{\text{EVO}}) \rho_1(t) \exp(i\tau H^{\text{EVO}}) \\
&= \sum_j -a_j 2S_Z I_Y^j \sin(k(\theta_{jS})t) [\cos^2(g(\theta_{jS})\tau) - \sin^2(g(\theta_{jS})\tau) \cos(4\phi_{jS})] \\
&\quad + a_j 2S_Z I_X^j \sin(k(\theta_{jS})t) \sin^2(g(\theta_{jS})\tau) \sin(4\phi_{jS}) \\
&\quad - a_j I_Z^j \sin(k(\theta_{jS})t) \sin(2g(\theta_{jS})\tau) \cos(2\phi_{jS})
\end{aligned} \tag{19}$$

where  $g(\theta_{jS}) = g\omega_D^j \sin^2(\theta_{jS})$ . After application of  $H^{\text{EVO}}$ , the terms proportional to  $I_{\pm}$  are removed by phase-cycling, leaving only the z-components of the density matrix. As before, the z-magnetization at the end of  $H^{\text{EVO}}$  is given by

$$\begin{aligned}
\langle I_Z(t, \tau) \rangle_0 &= \text{Tr}(\rho_0(t, \tau) I_Z) \\
&= \sum_j a_j \cos(k(\theta_{jS})t) \cos(2g(\theta_{jS})\tau)
\end{aligned} \tag{20}$$

$$\begin{aligned}
\langle I_Z(t, \tau) \rangle_1 &= \text{Tr}(\rho_1(t, \tau) I_Z) \\
&= \sum_j a_j \sin(k(\theta_{jS})t) \sin(2g(\theta_{jS})\tau) \cos(2\phi_{jS})
\end{aligned} \tag{21}$$

The  $\theta_{jS}$  dependence in both Eq. (20) and Eq. (21) could be cancelled if

$$\frac{3}{2}kt = \pm 2g\tau \quad (22)$$

Besides the trivial case ( $k = g = 0$ ), both of these equations cannot be satisfied simultaneously so only half of the signal can be made isotropic. However, if the  $\phi_{jS}$  dependence of Eq. (21) were absent, Eq. (20) and Eq. (21) could be added or subtracted to give  $\cos(k(\theta_{jS})t) \cos(2g(\theta_{jS})\tau) \pm \sin(k(\theta_{jS})t) \sin(2g(\theta_{jS})\tau) = \cos(k(\theta_{jS})t \mp 2g(\theta_{jS})\tau)$ , where the anisotropic portion of the signal can be removed [Eq. (22)].

The  $\phi_{jS}$  dependence in Eq. (21) can be removed by evolution under the Hamiltonians,  $H_{\pm 1}^{\text{DET}}$  given in Eq. (14). The pathway originating from  $\rho_0$  evolves for a time  $\tau_{\text{DET}}$  under  $H_1^{\text{DET}}$ . Next a filter is applied that only allows single-quantum coherences through as shown in Fig. 3. Finally  $H_1^{\text{DET}}$  is applied again for a time  $\tau_{\text{DET}}$ , the z-component of magnetization is measured to give the corresponding signal of

$$\begin{aligned} S_0 &= \text{Tr}[I_Z \rho_0(t, \tau, \tau_{\text{DET}})] \\ &= - \sum_j a_j \cos(k(\theta_{jS})t) \cos(2g(\theta_{jS})\tau) \sin^2(2f(\theta_{jS})\tau_{\text{DET}}) \end{aligned} \quad (23)$$

where  $f(\theta_{jS}) = f\omega_D^j \sin(2\theta_{jS})$ . Along the pathway originating from  $\rho_1$ , the system first evolves for a time  $\tau_{\text{DET}}$  under  $H_1^{\text{DET}}$ . Again a filter is applied that only allows single-quantum coherences through as shown in Fig. 3. Finally,  $H_{-1}^{\text{DET}}$  (instead of  $H_1^{\text{DET}}$ ) is applied for a time  $\tau_{\text{DET}}$ , and the z-component of magnetization is measured to give

$$\begin{aligned} S_1 &= \text{Tr}[I_Z \rho_1(t, \tau, \tau_{\text{DET}})] \\ &= \sum_j a_j \sin(k(\theta_{jS})t) \sin(2g(\theta_{jS})\tau) \sin^2(2f(\theta_{jS})\tau_{\text{DET}}) \cos^2(2\phi_{jS}) \end{aligned} \quad (24)$$

Assuming the  $\phi_{jS}$  angles are uniformly distributed over the interval  $[0, 2\pi]$  for each  $\theta_{jS}$ , Eq. (23) and Eq. (24) can be combined after powder averaging over  $\phi$  as follows:

$$\frac{1}{6\pi} \int_0^{2\pi} d\phi (S_0 \pm 2S_1) = - \sum_j a_j C_j(\tau_{\text{DET}}) [\cos(k(\theta_{jS})t \pm 2g(\theta_{jS})\tau)] \quad (25)$$

Eq. (25) requires only one of the solutions to Eq. (22) to be satisfied, thus completely removing the anisotropic portion of the signal. The corresponding signal intensities for spin  $j$ ,  $a_j C_j(\tau_{\text{DET}})$ ,

are given by

$$\begin{aligned}
a_j C_j(\tau_{\text{DET}}) &= \frac{a_j}{3} \left[ \frac{1}{2} \int_0^\pi d\theta_{jS} \sin(\theta_{jS}) \sin^2(2f\omega_D^j \sin(2\theta_{jS})\tau_{\text{DET}}) \right] \\
&= \frac{a_j}{6} \left[ 1 + \sum_{n=-\infty}^{\infty} \frac{J_{2n}(Z_j)}{16n^2 - 1} \right]
\end{aligned} \tag{26}$$

where  $Z_j = 4f\omega_D^j \tau_{\text{DET}}$ , and  $J_{2n}$  are spherical bessel functions. The signal intensity is a maximum when  $Z_j \approx 3.8$  with  $C \approx 0.24a_j$ , and  $C \rightarrow a_j/6$  as  $Z_j \rightarrow \infty$ .

### III. PULSE SEQUENCES

There exist two additional challenges in implementing the requisite Hamiltonians for the HETIE experiments over that of the HOMIE experiments. First of all, the homonuclear dipole-dipole interactions between the  $I$  spins (and the  $S$  spins if there is more than one present) must be removed, since the above theory deals only with a set of noninteracting  $I$  spins coupled to a single  $S$  spin. The second requirement is that the chemical shift anisotropy (CSA) of the  $I$  spins must also be removed. Since the heteronuclear dipolar coupling and the CSA of the  $I$  spins both have second-rank spatial components and are linear in the spin operator  $I_Z$ , they can only be separately manipulated by also applying pulses on the  $S$  spin.

Although there exist numerous ways to produce the necessary Hamiltonians for the HETIE method, one set of rotor-synchronized pulse sequences is shown in Fig. 4. These sequences represents a hybrid of the  $RN_n^\nu$  sequences<sup>20</sup> with the  $CN_n^\nu$  sequences<sup>21</sup>. The details of the sequences are given in Appendix A. The zeroth-order average Hamiltonians<sup>18</sup> for the sequences shown in Figure 4 are  $H$  [Fig. 4(A)],  $H^{\text{EVO}}$  [Fig. 4(B)],  $H_{+1}^{\text{DET}}$  [Fig. 4(C)], and  $H_{-1}^{\text{DET}}$  [Fig. 4(D)]. It worth pointing out that the  $\pi$ -pulse applied to the  $S$  spin is necessary in order to retain the heteronuclear coupling but to remove the CSA and chemical shift of the  $I$  spins.

For the case when  $\omega_{RF}^I = (15/2)\omega_r$ , the zeroth-order average Hamiltonian for the sequence shown in Fig. 4(A) is given by  $H$  [Eq. (12)], with  $k$  and  $k'$  given by

$$\begin{aligned}
k' &= \frac{4}{3\pi} \\
k &= \frac{4}{3\pi} \frac{3\cos^2(\theta_r) - 1}{2} \\
&= \bar{k} \frac{3\cos^2(\theta_r) - 1}{2}
\end{aligned} \tag{27}$$

For  $\omega_{\text{RF}}^{\text{EVO}} = (27/4)\omega_r$ , the sequence shown in Fig. 4(B) generates a zeroth-order Hamiltonian given by  $H^{\text{EVO}}$  [Eq. (13)], with  $g$  given by

$$\begin{aligned} g &= \cos\left(\frac{\pi}{4} - \frac{\pi}{2}\zeta_{\text{EVO}}\right) \cos(\pi\zeta_{\text{EVO}}) \frac{\sin^2(\theta_r)}{2\pi[4\zeta_{\text{EVO}}^2 - 1]} \\ &= \bar{g} \sin^2(\theta_r) \end{aligned} \quad (28)$$

where  $\zeta_{\text{EVO}} = \omega_r/\omega_{\text{RF}}^{\text{EVO}}$ .

Finally, for  $\omega_{\text{RF}}^{\text{DET}} = (15/2)\omega_r$ , the sequences shown in Figures 4(C) and 4(D), produce zeroth-order Hamiltonians given respectively by  $H_1^{\text{DET}}$  and  $H_{-1}^{\text{DET}}$  [Eq. (14)], with  $f$  given by

$$\begin{aligned} f &= \frac{\cos\left(\frac{\pi}{4}\right) \sin(2\theta_r) \cos\left(\frac{\pi}{4} - \frac{\pi}{4}\zeta_{\text{DET}}\right) \cos\left(\frac{\pi}{2}\zeta_{\text{DET}}\right)}{\pi[\zeta_{\text{DET}}^2 - 1]} \\ &= \bar{f} \sin(2\theta_r) \end{aligned} \quad (29)$$

Note that in order to create the same  $\bar{f}$  dependence in both  $H_{-1}^{\text{DET}}$  as in  $H_1^{\text{DET}}$ , the order of the composite  $180^\circ$  pulses had to be switched, as shown in Fig. 4(D).

To simplify the experiment, a solution can be found for a single rotor axis. Under this condition, the evolution must satisfy

$$\begin{aligned} &\left| \frac{\omega_D}{t + \tau} \left( \bar{k}t \frac{(3\cos^2(\theta_r) - 1)}{2} \frac{(3\cos^2(\theta) - 1)}{2} \pm 2\bar{g}\tau \sin^2(\theta_r) \sin^2(\theta) \right) \right| \\ &= \left| \frac{k\omega_D t}{(t + \tau)} \right| = \sigma\omega_D \end{aligned} \quad (30)$$

When  $\theta_r \neq 0^\circ$ ,  $t$  and  $\tau$  must both be a multiple of the rotor period. In addition,  $H_{\pm 1}^{\text{DET}}$  must be nonzero at the given rotor axis, which means solutions near  $90^\circ$  and  $0^\circ$  must be discarded due to the  $\sin(2\theta_r)$  dependence in Eq. (29). From Eq. (30), the rotor angle,  $\theta_r$ , that the sample must be spun at in order to remove the anisotropy is given by

$$\theta_r = \arccos\left(\sqrt{\frac{3\bar{k}t \pm 8\bar{g}\tau}{9\bar{k}t \pm 8\bar{g}\tau}}\right) \quad (31)$$

#### IV. EXPERIMENT

An experimental implementation of HETIE was tested on a natural abundance sample of ferrocene ( $\text{Fe}(\text{C}_5\text{H}_5)_2$ ) which was doped with 2% by weight cobaltocene ( $\text{Co}(\text{C}_5\text{H}_5)_2$ ) in order to shorten the  $T_1$  relaxation time of the ferrocene protons from 60 s to 1 s. The sample was prepared

by melting the two compounds together, and the resulting mixture was ground to a powder and packed into a 4 mm MAS rotor. The experiment was performed at a  $^1\text{H}$  resonance frequency of 300.986 MHz, exactly on resonance for the protons of ferrocene. For  $t = \tau$ , and using the sequences shown in Fig. 4, a rotor angle of  $\theta_r = 73.9^\circ$  was used [Eq. (31)]. The angle was set externally to  $73.9^\circ \pm 0.2^\circ$  with the use of a protractor and a long rod which was exactly coaxial with the spinning axis. The  $^1\text{H}$  spectrum obtained under the conditions of the HETIE experiment is shown in Figure 5. The  $^1\text{H}$  linewidth is 5.6 kHz and is clearly not isotropic due to the  $^1\text{H}$ - $^1\text{H}$  dipolar couplings and the  $^1\text{H}$  CSA which are only scaled when spinning at 15 kHz at  $\theta_r = 73.9^\circ$ .

The spectrometer used in these experiments was an Infinity-plus spectrometer (Varian Inc., Palo Alto, CA). A Chemagnetics (now Varian Inc., Palo Alto, CA) 4mm Apex-HX MAS probe was used. The RF amplitudes for the sequence were calibrated by finding the maximum intensity of the required  $\frac{\pi}{2}$ -pulse on proton. The  $\pi$ -pulse on  $^{13}\text{C}$  was calibrated using cross-polarization and observing where the cross-polarized signal's phase was inverted after the application of a fixed  $\pi$ -pulse. The pulse sequence was rotor synchronized by controlling the spinning speed at  $\omega_r/(2\pi) = 15 \text{ kHz} \pm 3 \text{ Hz}$ .

One of the difficulties with implementing the HETIE sequence was keeping the requirements of RF and rotor synchronization within experimental limitations. The specific experimental limitations that had to be dealt with were the fact that the probe could only spin the sample up to 20 kHz, and the maximum achievable RF power was  $\omega_{\text{RF}}/(2\pi) = 150 \text{ kHz}$ . In the experiments used in the HETIE sequence, the spinning speed usually set the ceiling for the maximum RF power used in the experiment. Although an RF power of 150 kHz could be produced, the RF pulse quality diminished with increasing RF power. For this reason, better performance was often achieved at RF powers of approximately 100 kHz, which was the RF used in the HETIE experiments below.

## V. RESULTS AND DISCUSSION

The sequences shown in Fig. 4 for  $t = \tau$  yields a scaling factor of  $\sigma = 0.0817$  [Eq. (30)]. Although ferrocene is an ideal sample due to the scaled dipolar couplings and high molecular symmetry, there exist more than 30 different structures in the Cambridge Structure Database with C-H bond lengths varying in the range of 0.99 to 1.1 Å. We have restricted our analysis of the bond lengths to more modern neutron diffraction studies where the diffraction method has a better chance of detecting the proton positions. In an attempt to predict the expected values for the

observed scaled couplings, the bond lengths were taken from the neutron structure with the best experimental parameters<sup>22</sup>. In these studies, the complex Cp motions were taken into account in the diffraction analysis. This analysis gave a variable interpretation of the carbon-proton internuclear distances (standard deviation = 0.02 Å) for room temperature samples of ferrocene. We used the structure found in the Cambridge Structure Database (CSD ref. #FEROCE29) which reports C-H distances of 1.04, 2.18, and 3.28 Å within the Cp ring. In addition to the work by Brock et al.<sup>22</sup>, there has been much discussion on the proper interpretation of the ferrocene diffraction data<sup>23</sup>, and we hope that NMR might be able to provide some additional insight.

The only C-H couplings considered are those located within the Cp ring of the ferrocene, since the other protons are much farther away with couplings reduced by the fast motion of the Cp ring. The ring motion also affects the observable couplings since the motional timescale is much greater than that of the coupling strengths; the molecular motion scales the observed couplings by a factor  $P_2[\cos(\theta)]$ , where  $\theta$  is the angle between the C-H vector and the axis of fast motion. For the case of rotation about the Cp axis, the observed couplings are scaled by  $P_2[\cos(90^\circ)] = -1/2$ .

It is important to consider the uncertainties in the C-H distance when comparing the theoretical and experimental dipolar coupling results. Using the neutron diffraction data<sup>22</sup> and the associated standard deviation from the different analyses of the same diffraction data, we expect the unique observed dipolar couplings of room temperature ferrocene between a single  $^{13}\text{C}$  on the ring and the protons as scaled by the HETIE experiment to be  $1026 \pm 232$ ,  $111.5 \pm 12$ ,  $33 \pm 2.4$  Hz. The error in these scaled couplings may seem quite large; however, the  $\frac{1}{r^3}$  dependence of the coupling amplifies errors at small distances.

These scaled coupling values are determined from the ideal scaling factor,  $\sigma = 0.0817$ , which lacks any inclusion of interactions or higher-order terms in the average Hamiltonian which might degrade the performance of the sequence in addition to possible pulse and phase errors. Exact numerical simulations were performed on a three spin,  $I_2S$  system, where only the two closest protons to the  $^{13}\text{C}$  in the Cp ring were considered. The simulations shown in Fig. 7 were performed with a weak homonuclear interaction (A) without and (B) with a proton CSA. As is shown in Figure 7(A), the peaks are isotropic and at the correct frequencies (as determined from the scaling factor,  $\sigma = 0.0817$ ). It should be noted that since the spectral range is determined by the spinning speed divided by the number of evolution units per dwell (15/8 kHz), the largest C-H coupling is actually under-sampled and is effectively folded in from the edges of the spectrum. This is an unfortunate artifact; however it is necessary given our maximum RF restrictions and

spinning speeds. Smaller couplings, which are expected to be of greatest interest for structure determinations, will typically be within the spectral window given by the current experimental constraints.

Figure 7(B) shows the results of a simulation on a more realistic sample with non-zero Euler angles relating the axes of the interactions, as well as a 5 kHz CSA on each of the protons. Fig. 7(B) indicates that the weaker coupling peaks are virtually unaffected while the larger coupling peaks have some additional broadening which we attribute to a higher-order cross-term in the average Hamiltonian between the CSA and the heteronuclear dipolar coupling, since the underlying heteronuclear dipolar coupling is significantly larger. The CSA values used in Fig. 7(B) is in excess of what has previously been seen for the CSA of protons in ferrocene<sup>24</sup> with a  $\Delta\sigma(= \sigma_{\parallel} - \sigma_{\perp})$  of  $-6.5 \pm 0.1$  ppm. In addition, further numerical simulations using typical values for heteronuclear scalar J couplings showed that the signal is not sensitive to J couplings, even with the inclusion of the CSA.

Finally, Figure 8 shows a comparison between (A) an ideal simulation and (B) the actual experimental signal. The first thing to note is that the spectrum of Figure 8 (B) is a power spectrum ( $|f(\omega)|^2$ ) which is necessary to facilitate the comparison with the simulation, since the signal to noise was quite low. Secondly, there appears to be a large zero peak in the experimental spectrum which has been truncated so that the peaks of interest are more clearly displayed. The origin of this peak is somewhat uncertain; however we suspect that it is related to the signal decay caused by the accumulation of pulse and phase errors, but this requires further investigation.

The largest coupling peaks in the experimental spectrum appear to be close to the correct frequencies (minus the spectral folding) at  $1090 \pm 10$  Hz, which corresponds to a bond distance of  $1.019 \pm 0.003 \text{ \AA}$ . The next largest coupling peaks occur at  $147 \pm 10$  Hz, which correspond to a distance of  $1.99 \pm 0.041 \text{ \AA}$ , which is different from the neutron diffraction distance of  $2.18 \text{ \AA}$  as shown in Figure 8. The smallest C-H coupling peak can not be observed unless the large zero peak is deconvolved, which is shown in Fig. 9. The peaks roughly occur at  $31.5 \pm 15$  Hz, which corresponds to a distance of  $3.52 \pm 0.60 \text{ \AA}$ , which is within the range of the neutron diffraction distance of  $3.28 \text{ \AA}$ .

The HETIE method can provide a valuable complement to existing methods in solid-state structure determination. Consider determining the structure of an  $I_3S$  system as shown in Figure 10. The HETIE method provides information about the heteronuclear bond distances in a powdered sample (D1S, D2S, and D3S in Figure 10). If either the angles between the various heteronu-

clear dipolar vectors could be determined ( $\theta_{12}$ ,  $\theta_{23}$ ,  $\theta_{13}$ ) or the homonuclear distances ( $D_{12}$ ,  $D_{13}$ ,  $D_{23}$ ), then the structure of the system would be determined. Determining all the homonuclear distances for an abundant spin species such as  $^1\text{H}$  is problematic in solids, since extracting the dipolar couplings becomes almost impossible due to the increasing spectral complexity with increasing number of I spins. However, there exists a variety of methods which in principle could provide the angles between the heteronuclear dipolar vectors by performing either dipole-dipole correlation experiments or dipole-CSA correlations<sup>25–27</sup>. In addition, coupling the HETIE method with Dynamic Angle Spinning (DAS) techniques<sup>28</sup> can not only improve the scaling factor  $\sigma$  of the HETIE experiment, but also correlations between the isotropic heteronuclear couplings and the isotropic chemical shifts could be obtained (Appendix B). In the future, application of HETIE along with these correlation techniques may help to solve structural problems in the solid-state which are not amenable to current methodologies.

## VI. CONCLUSIONS

A new methodology, HETeronuclear Isotropic Evolution (HETIE), was presented which produces isotropic proton-detected local-field spectra of powdered samples. HETIE works by removing the anisotropic portion of the heteronuclear dipolar coupling frequency by having the system evolve under carefully designed Hamiltonians and evolution pathways. In this paper, HETIE was shown both theoretically and experimentally to produce linear, isotropic, proton-detected local field spectra. The heteronuclear coupling values as determined by the HETIE experiment on a ferrocene sample actually agree quite well with the ‘known structure’, given the uncertainties in the interpretation of ferrocene diffraction studies. Thus far we have made only a single study, but with additional refinement of the HETIE sequence, we anticipate this method may yield valuable structural insight into many solid-state systems.

## Acknowledgments

We would like to thank Dr. W.B. Blanton for useful discussions on the HETIE method. R.H.H. acknowledges the National Science Foundation for a predoctoral fellowship during the course of this work. This work was supported by the Director, Office of Science, Office of Basic Energy Sciences, Materials Sciences and Engineering Division, of the U.S. Department of Energy (Contract

- \* R.H.H. and J.D.W. contributed equally to this work.; Current Address: National Institutes of Health, Bethesda, Maryland
- † R.H.H. and J.D.W. contributed equally to this work.; Current Address: Department of Chemistry and Chemical Biology, Harvard University, Cambridge, Massachusetts
- ‡ Corresponding author: [pinest@cchem.berkeley.edu](mailto:pinest@cchem.berkeley.edu)
- <sup>1</sup> D. E. Wemmer, *Method Enzymol.* **309**, 536 (1999).
  - <sup>2</sup> D. D. Laws, H. M. L. Bitter, K. Liu, H. L. Ball, K. Kaneko, H. Wille, F. E. Cohen, S. B. Prusiner, A. Pines, and D. E. Wemmer, *Proc. Natl. Acad. Sci. USA* **98**, 11686 (2001).
  - <sup>3</sup> J. van Beek, L. Beaulieu, H. Schafer, M. Demura, T. Asakura, and B. Meier, *Nature* **405**, 1077 (2000).
  - <sup>4</sup> R. Tycko, *Prog. Nucl. Magn. Res. SP* **42**, 53 (2003).
  - <sup>5</sup> R. H. Havlin and R. Tycko, submitted (2004).
  - <sup>6</sup> J. M. Griffiths and R. G. Griffin, *Anal. Chim. Acta.* **283**, 1081 (1993).
  - <sup>7</sup> D. P. Weitekamp, A. Bielecki, D. B. Zax, K. Zilm, and A. Pines, *Phys. Rev. Lett.* **50**, 1807 (1983).
  - <sup>8</sup> D. B. Zax, A. Bielecki, K. W. Zilm, A. Pines, and D. P. Weitekamp, *J. Chem. Phys.* **83**, 4877 (1985).
  - <sup>9</sup> R. Tycko, *J. Magn. Reson.* **75**, 193 (1987).
  - <sup>10</sup> R. Tycko, *Phys. Rev. Lett.* **60**, 2734 (1988).
  - <sup>11</sup> R. Tycko, *J. Chem. Phys.* **92**, 5776 (1990).
  - <sup>12</sup> B. Q. Sun and A. Pines, *J. Magn. Reson. A* **109**, 157 (1994).
  - <sup>13</sup> M. Hong, K. Schmidt-rohr, and A. Pines, *J. Am. Chem. Soc.* **117**, 3310 (1995).
  - <sup>14</sup> S. Caldarelli, M. Hong, L. Emsley, and A. Pines, *J. Phys. Chem.* **100**, 18696 (1996).
  - <sup>15</sup> D. McElheny, E. DeVita, and L. Frydman, *J. Magn. Reson.* **143**, 321 (2000).
  - <sup>16</sup> J. Grinshein, C. V. Grant, and L. Frydman, *J. Am. Chem. Soc.* **124**, 13344 (2002).
  - <sup>17</sup> J. D. Walls, W. B. Blanton, R. H. Havlin, and A. Pines, *Chem. Phys. Lett.* **363**, 372 (2002).
  - <sup>18</sup> U. Haeberlen and J. S. Waugh, *Phys. Rev.* **175**, 453 (1968).
  - <sup>19</sup> J. S. Waugh, L. M. Huber, and U. Haeberlen, *Phys. Rev. Lett.* **20**, 180 (1968).
  - <sup>20</sup> M. Carravetta, M. Eden, X. Zhao, A. Brinkmann, and M. H. Levitt, *Chem. Phys. Lett.* **321**, 205 (2000).
  - <sup>21</sup> Y. K. Lee, N. D. Kumur, M. Helmle, O. G. Johannessen, N. C. Nielsen, and M. H. Levitt, *Chem. Phys. Lett.* **242**, 304 (1995).

- <sup>22</sup> C. P. Brock and Y. Fu, Acta Cryst. **B53**, 928 (1997).
- <sup>23</sup> D. Braga, Chem. Rev. **92**, 633 (1992).
- <sup>24</sup> H. W. Spiess, H. Zimmermann, and U. Haeberlen, Chem. Phys. **12**, 123 (1976).
- <sup>25</sup> M. Linder, A. Hohener, and R. R. Ernst, J. Chem. Phys. **73**, 4959 (1980).
- <sup>26</sup> A. Ramamoorthy, C. Wu, and S. Opella, J. Magn. Reson. Ser. B **107**, 88 (1995).
- <sup>27</sup> A. Ramamoorthy and S. J. Opella, Solid State Nucl. Magn. **4**, 387 (1995).
- <sup>28</sup> K. T. Mueller, B. Q. Sun, G. C. Chingas, J. W. Zwanziger, T. Terao, and A. Pines, J. Magn. Reson. **86**, 470 (1990).
- <sup>29</sup> P. Madhu, X. Zhao, and M. Levitt, Chem. Phys. Lett. **346**, 142 (2001).
- <sup>30</sup> A. Brinkmann, M. Eden, and M. H. Levitt, J. Chem. Phys. **112**, 8539 (2000).
- <sup>31</sup> M. Bak, J. T. Rasmussen, and N. C. Nielsen, J. Magn. Reson. **147**, 296 (2000).

## APPENDIX A: PULSE SEQUENCE DETAILS

The Hamiltonian for an  $I_N S$  under mechanical rotation and RF irradiation is given by

$$\begin{aligned} H_{\text{sys}} &= H_{II}(t) + H_{IS}(t) + H_I(t) + H_S(t) + H_{RF}^I(t) \\ &= H_{INT}(t) + H_{RF}^I(t) \end{aligned} \quad (\text{A1})$$

where the equations and forms for the various terms in  $H_{\text{sys}}$  are given in Eqs. (6)-(9). The basic Hamiltonians needed for the HETIE method require finding a particular  $H_{RF}^I(t)$  such that the spin system appears to evolve, in some averaged sense, under  $H$  [Eq. (12)],  $H^{\text{EVO}}$  [Eq. (13)], and  $H_{\pm}^{\text{DET}}$  [Eq. (14)]. Transforming into an interaction frame defined by  $H_{RF}^I(t)$ , the propagator,  $U(t_1, t_0)$ , can be written as

$$\begin{aligned} U(t_1, t_0) &= T \exp \left( -i \int_{t_0}^{t_1} dt' H_{\text{sys}}(t') \right) \\ &= V(t_1, t_0) T \exp \left( -i \int_{t_0}^{t_1} dt' \hat{H}_{\text{INT}}(t') \right) \end{aligned} \quad (\text{A2})$$

where  $T$  is the Dyson time ordering operator and

$$V(t_1, t_0) = T \exp \left( -i \int_{t_0}^{t_1} dt' H_{RF}^I(t') \right) \quad (\text{A3})$$

$$\hat{H}_{\text{INT}}(t) = V^\dagger(t, t_0) [H_{II}(t) + H_{IS}(t) + H_I(t) + H_S(t)] V(t, t_0) \quad (\text{A4})$$

For short enough times, the propagator in Eq. (A2) can be approximated as

$$U(t_1, t_0) = V(t_1, t_0) \exp(-it\bar{H}) \quad (\text{A5})$$

where  $t = t_1 - t_0$ , and  $\overline{H}$  is the average Hamiltonian<sup>18</sup> over the time interval  $t$ .  $\overline{H}$  is given by

$$\overline{H} = \sum_{n=0}^{\infty} \overline{H}^{(n)} \quad (\text{A6})$$

where  $\overline{H}^{(n)}$  is the  $n$ th order average Hamiltonian. The zeroth- ( $\overline{H}^{(0)}$ ) and first-order ( $\overline{H}^{(1)}$ ) average Hamiltonians are explicitly given by

$$\overline{H}^{(0)} = \frac{1}{t} \int_{t_0}^{t_1} dt' \hat{H}_{\text{INT}}(t') \quad (\text{A7})$$

$$\overline{H}^{(1)} = -\frac{i}{2t} \int_{t_0}^{t_1} \int_{t_0}^{t'} dt' dt'' [\hat{H}_{\text{INT}}(t'), \hat{H}_{\text{INT}}(t'')] \quad (\text{A8})$$

In the following, the aim will be to create zeroth-order average Hamiltonians,  $\overline{H}^{(0)}$ , which are equal to  $H$ ,  $H^{\text{EVO}}$ , and  $H_{\pm 1}^{\text{DET}}$ .

The set of pulse sequences that were used to create  $H$ ,  $H^{\text{EVO}}$ , and  $H_{\pm 1}^{\text{DET}}$  while removing both the CSA and homonuclear dipolar interactions are shown in Fig. 4. Each of these pulse sequences are composed of small blocks given by

$$[(\pi/2)_X - (\pi/2)_Y - (\pi/2)_X]_{\phi} [(\pi/2)_Y - (\pi/2)_X - (\pi/2)_Y]_{\phi_1} \quad (\text{A9})$$

The sequence in Eq. (A9) has the advantage of being able to remove the homonuclear dipolar coupling between the  $I$  spins<sup>29</sup>. The propagator for the block in Eq. (A9) can be approximated by

$$U(t) \approx \exp(-2i[\phi_1 - \phi]I_Z) \exp(-it_{\text{cyc}}\overline{H}^{(0)}) \quad (\text{A10})$$

where  $t_{\text{cyc}} = [3\pi/(\omega_{RF})]$  is the total time for the block of pulses, and  $\overline{H}^{(0)}$  is the zeroth-order average Hamiltonian over the time  $t_{\text{cyc}}$ , calculated using Eq. (A7).  $\overline{H}^{(0)}$  can be written as

$$\overline{H}^{(0)} = \sum_r \sum_n \sum_m \sum_{k=-m}^m \sum_{p=-n}^n b_{k,p}^{m,n} A_{m,k}^r T_{n,p}^r \quad (\text{A11})$$

where  $A_{m,k}^r$  are spatial tensors of rank  $m$ , and  $T_{n,p}^r$  are spin tensors or rank  $n$  in the  $I$  space (i.e., both  $I_Z$  and  $I_Z S_Z$  are first rank tensors in the  $I$  space, whereas  $3I_Z^i I_Z^j - \vec{I}^i \cdot \vec{I}^j$  is a second rank tensor in the  $I$  space). The sum over  $r$  denotes different terms in  $\overline{H}^{(0)}$  with the same values for  $k$ ,  $p$ ,  $m$ , and  $n$  (for example,  $\omega_{\text{CSA}}^1 A_{2,0}^1 I_Z^1$  and  $\omega_D^{S1} A_{2,0}^{S1} I_Z^1 S_Z$  each have  $k = 0$ ,  $p = 0$ ,  $m = 2$ , and  $n = 1$ ).

The coefficients,  $b_{k,\pm 1}^{2,1}$  (in front of terms like  $I_{\pm}^j$  and  $I_{\pm}^j S_Z$ ) are given by

$$\begin{aligned} b_{k,\pm 1}^{2,1} &= -d_{k,0}^2(\theta_r) v_k^{\frac{3}{2}} \exp(\mp i\phi) \exp\left(\pm i\frac{\pi}{4}\right) (\exp(\mp i[\phi - \phi_1]) v_k^3 - 1) \\ &\times \cos\left(\frac{\pi}{4} \mp \frac{\pi k \zeta}{4}\right) \cos\left(\frac{\pi k \zeta}{2}\right) \frac{2}{3\pi[(k\zeta)^2 - 1]} \end{aligned} \quad (\text{A12})$$

where  $d_{k,0}^2(\theta_r)$  is the reduced Wigner matrix element,  $\theta_r$  is the angle that the rotor axis makes with respect to the Zeeman field,  $\eta = \omega_r/\omega_{RF}$ , and  $v_k = \exp[i(k\zeta\pi)/2]$ . The coefficients  $b_{k,\pm 1}^{2,2}$  (in front of terms like  $I_Z^i I_{\pm}^j + I_{\pm}^i I_Z^j$ ) are given by

$$b_{k,\pm 1}^{2,2} = 2d_{k,0}^2(\theta_r) \exp(\mp i\phi) v_k^{\frac{3}{2}} \exp\left(\mp i\frac{\pi}{4}\right) [v_k^3 \exp(\mp i[\phi - \phi_1]) + 1] \\ \times \cos\left(\frac{\pi}{4} \pm \frac{\pi k\zeta}{2}\right) \cos\left(\frac{\pi k\zeta}{4}\right) \frac{1}{\pi[4 - (k\zeta)^2]} \quad (\text{A13})$$

Note that when  $v_k^3 \exp(\pm i[\phi - \phi_1]) = 1$ ,  $b_{k,\pm 1}^{2,1} = 0$  while  $b_{k,\pm 1}^{2,2} \neq 0$ , and when  $v_k^3 \exp(\pm i[\phi - \phi_1]) = -1$ ,  $b_{k,\pm 1}^{2,1} \neq 0$  while  $b_{k,\pm 1}^{2,2} = 0$ . This is due to the fact that the units  $[(\pi/2)_X(\pi/2)_Y(\pi/2)_X]$  and  $[(\pi/2)_Y(\pi/2)_X(\pi/2)_Y]$  act like composite  $180^\circ$  pulse (with an additional Z rotation). Under a  $180^\circ$  X pulse,  $I_{\pm} \rightarrow I_{\mp}$ , while  $I_Z^i I_{\pm}^j + I_{\pm}^i I_Z^j \rightarrow -(I_Z^i I_{\mp}^j + I_{\mp}^i I_Z^j)$ , hence the ability of these sequences to distinguish between odd and even ranked spin tensors. This is part of the basis for the  $RN_v^\eta$  sequences which have been used extensively in solid-state NMR<sup>20</sup>. Note also that  $b_{0,k}^{0,1} = b_{0,k}^{2,1} = 0$  for  $k = 0, \pm 1$ , and  $b_{0,0}^{2,0} = 0$ , so that these sequences are also compensated for isotropic chemical shifts and the  $T_{2,0}^{ij}$  component of the homonuclear dipolar interaction in the RF interaction frame.

The extra Z rotation of phase  $\Delta = 2[\phi_1 - \phi]$  in Eq. (A10) propagates throughout the sequence by repeatedly applying the basic unit while the sample is being mechanically rotated. Defining the operator for a rotation of an angle  $\phi$  about the  $\hat{z}$ -axis as  $P_Z(\phi) = \exp[-i\phi I_Z]$ , the propagator over  $N$  applications of the basic unit is given by

$$U(N\tau_{cyc}, 0) = T \prod_{w=1}^N P_Z(\Delta) \exp\left(-i\tau_{cyc} \overline{H}_w^{(0)}\right) \quad (\text{A14})$$

where  $\overline{H}_w^{(0)}$  is the zeroth-order average Hamiltonian over the  $w$ th application of the sequence in Eq. (A9). Since the sample is being mechanically rotated during the pulse sequence,  $\overline{H}_w^{(0)}$  is not equal to  $\overline{H}^{(0)}$  in Eq. (A11), since the coefficients of the spatial tensors in  $H_{\text{INT}}(t)$  are time-dependent [Eq. (10)] and the length of the pulse sequence in Eq. (A9) is in general not equal to a multiple of the rotor period.  $\overline{H}_w^{(0)}$  is given by

$$\overline{H}_w^{(0)} = \sum_r \sum_n \sum_m \sum_{k=-m}^m \sum_{p=-n}^n b_{k,p}^{m,n} (\nu_k)^{w-1} A_{m,k}^r T_{n,p}^r \quad (\text{A15})$$

where  $\nu_k = \exp(ik\omega_r\tau_{cyc})$  with  $\tau_{cyc}$  being the time of the given pulse sequence (in the case of Eq. (A9),  $\tau_{cyc} = 3\pi/\omega_{RF}$ ).

If  $N\Delta = 2\pi q$  where  $q$  is some integer, an average Hamiltonian for the whole propagator,

$U(N\tau_{cyc}, 0)$  in Eq. (A14), can be calculated as follows:

$$\begin{aligned} U(N\tau_{cyc}, 0) &\approx P_Z(N\Delta) T \prod_{w=1}^N \exp \left[ -i\tau_{cyc} P_Z^\dagger([w-1]\Delta) \bar{H}_w^{(0)} P_Z([w-1]\Delta) \right] \\ &\approx \exp \left( -iN\tau_{cyc} \bar{\bar{H}}^{(0)} \right) \end{aligned} \quad (\text{A16})$$

where  $\bar{\bar{H}}^{(0)}$  is the zeroth-order average Hamiltonian over the whole sequence, which is given by

$$\begin{aligned} \bar{\bar{H}}^{(0)} &= \frac{1}{N\tau_{cyc}} \sum_{w=1}^N \tau_{cyc} P_Z^\dagger([w-1]\Delta) \bar{H}_w^{(0)} P([w-1]\Delta) \\ &= \sum_r \sum_n \sum_m \sum_{k=-m}^m \sum_{p=-n}^n A_{m,k}^r T_{n,p}^r \left[ \frac{1}{N} \sum_{w=0}^{N-1} \exp(iw[p\Delta + k\omega_r\tau_{cyc}]) \right] \end{aligned} \quad (\text{A17})$$

For  $\Delta = 2\pi\nu/N$  and  $\omega_r\tau_{cyc} = 2\pi\eta/N$ , only those terms of the form  $A_{m,k}^r T_{n,p}^r$  with  $k$  and  $p$  satisfying

$$k\eta + p\nu = NZ \quad (\text{A18})$$

where  $Z$  is an integer, will be present to lowest order, since

$$\frac{1}{N} \sum_{k=0}^{N-1} \exp\left(i\frac{2\pi Q}{N}\right) = 1 \quad (\text{A19})$$

if  $Q = NZ$  with  $Z$  an integer and equals zero in all other cases. This is basis for the  $CN_\nu^\eta$  sequences<sup>21,30</sup>.

The first-half of the sequence (before the 180° pulse on the  $S$  spin) in Figure 4(A) is comprised of two blocks of pulses of the form given in Eq. (A9) with  $\phi = \pi$  and  $\phi_1 = 0$ , which are phase shifted by 90° from each other. This unit is then repeated five times which makes, according to Eq. (A18), the whole sequence formally equivalent to  $C5_0^2$  when  $\omega_{RF} = (15/2)\omega_r$ . In this case, only those terms of the form  $A_{m,0}^r T_{n,p}^r$  will contribute to  $\bar{\bar{H}}^{(0)}$ . As discussed earlier, for sequences of the form of Eq. (A9), the coefficients  $b_{0,0}^{m,n}$  for terms of the form  $A_{m,0}^r T_{n,0}^r$  are zero and thus do not contribute to  $\bar{\bar{H}}^{(0)}$ . Additionally, because of the concatenation of two sequences which are phase shifted by  $\pi/2$  from each other, terms of the form  $A_{m,0}^r T_{2,\pm 2}^r$  will cancel and thus not contribute to  $\bar{\bar{H}}^{(0)}$ . Finally since  $\exp(-i(\phi_1 - \phi)) = -1$ , terms of the form  $A_{m,0}^r T_{2,\pm 1}^r$  also will not contribute [Eq. (A13)], leaving only terms of only of the form  $A_{m,0}^r T_{1,\pm 1}^r$  to contribute to  $\bar{\bar{H}}^{(0)}$  [Eq. (A12)], which includes terms arising from both the CSA ( $I_\pm$ ) and heteronuclear couplings ( $I_\pm S_Z$ ). In

order to distinguish between these two contributions, the sequence is repeated again with all the phases of the pulses shifted by  $180^\circ$  in addition to applying a  $180^\circ$  pulse to the  $S$  spin. This has the effect of refocussing the CSA terms but keeping the heteronuclear coupling terms. Such a pulse sequence motif is used in all the sequences shown in Figure 4. The average Hamiltonian for the sequence in Figure 4(A) is  $H$  [Eq. (12)].

The sequence shown in Figure 4(B) is formally equivalent to a  $C9_5^2$  sequence when  $\omega_{RF} = (27/4)\omega_r$ , which again lets through terms of the form  $A_{2,\pm 2}^r T_{n,\pm 1}^r$  from Eq. (A18) (the terms of the form  $A_{m,0}^r T_{n,0}^r$  do not contribute due to the basic pulse blocks [Eq. (A9)]). Due to Eq. (A12) and Eq. (A13), only terms of the form  $A_{2,\pm 2}^r T_{1,\pm 1}^r$  contribute. The average Hamiltonian for the sequence in Figure 4(B) is  $H^{\text{EVO}}$  [Eq. (13)].

Finally, the sequences shown in Figure 4(C) [formally equivalent to  $C5_8^2$ ] and 4(D) [formally equivalent to  $C5_{12}^2$ ] generate average Hamiltonians  $H_1^{\text{DET}}$  and  $H_{-1}^{\text{DET}}$  respectively when  $\omega_{RF} = (15/2)\omega_r$ . Both sequences  $C5_8^2$  and  $C5_{12}^2$  let through terms of the form  $A_{m,0}^r T_{n,0}^r$  [Eq. (A18)], but the basic blocks [Eq. (A9)] prevent such terms from contributing to  $\bar{H}^{(0)}$ . Using Eq. (A18), the sequence in Fig. 4(C) also lets through terms of the form  $A_{2,\pm 2}^r T_{2,\pm 2}^r$  (which are removed removed by concatenating two pulse sequence blocks which are phase shifted by  $90^\circ$  relative to each other) and  $A_{2,\pm 1}^r T_{n,\pm 1}^r$ . Due to Eq. (A12) and Eq. (A13), only terms of the form  $A_{2,\pm 1}^r T_{1,\pm 1}^r$  contribute to  $\bar{H}^{(0)}$ . Using Eq. (A18), the sequence in Fig. 4(D) lets through terms of the form  $A_{2,\pm 2}^r T_{2,\mp 2}^r$  (which are removed removed by concatenating two pulse sequence blocks which are phase shifted by  $90^\circ$  relative to each other) and  $A_{2,\pm 1}^r T_{n,\mp 1}^r$ . Due to Eq. (A12) and Eq. (A13), only terms of the form  $A_{2,\pm 1}^r T_{1,\mp 1}^r$  contribute to  $\bar{H}^{(0)}$ . Note that the order of the two composite  $180^\circ$  pulses are switched in the sequence in Figure 4(D) relative to those in Figure 4(C). This is to ensure that the scaling factor  $\bar{f}$  [Eq. (29)] is the same for both sequences.

## APPENDIX B: IDEAL HETIE SEQUENCE WITH OPTIMAL SCALING FACTOR $\sigma$

In trying to obtain the maximal scaling factor  $\sigma$ , all sequences used to generate the various Hamiltonians ( $H$ ,  $H^{\text{EVO}}$ , and  $H_{\pm}^{\text{DET}}$ ) are assumed to be comprised of delta pulses (i.e., unlimited RF power can be used). Additionally, the sample is allowed to switch between different rotor angles during the course of the experiment. The optimal sequences to produce  $H$  and  $H^{\text{EVO}}$  for a single  $IS$  spin system will now be presented.

While spinning the sample at  $\theta_r = 0^\circ$  for a total time  $t = 4Nt''$ , the sequence

$$(\pi/2)_{\pi/2}^I - (t'' - (\pi)_0^I(\pi)_0^S - 2t'' - (\pi)_\pi^I(\pi)_\pi^S - t'')^N - (\pi/2)_{3\pi/2}^I \quad (\text{B1})$$

produces an average Hamiltonian,  $H$ , with  $k = k' = 1$  [Eq. (12)].

$H^{\text{EVO}}$  [Eq. (13)] can be created by a variety of rotor-synchronized RF pulse sequences, each resulting in a different scaling factor,  $g$ . A maximal scaling can be achieved for  $g$  by applying  $N$ , phase-incremented, rotor-synchronized units, with the  $k^{\text{th}}$  unit given by

$$[(\pi/2)_0 - \tau_d - (\pi/2)_\pi]_{\phi_k} \quad (\text{B2})$$

where  $\tau_d = 2\pi/(\omega_r N)$  and  $\phi_k = 4\pi/N$ . The sequence in Eq. (B2) is then repeated with an extra  $\pi$  phase shifted added to the pulses and is sandwiched between two  $180^\circ$  pulses on the  $S$  spin. This helps to refocus the CSA terms while keeping the heteronuclear couplings to lowest order. Spinning the rotor at an angle  $\theta_r$  and applying the above sequence creates an average Hamiltonian given by  $H^{\text{EVO}}$  with  $g$  given by

$$g = \frac{3N \sin^2(\theta_r)}{32\pi} \sin\left(\frac{2\pi}{N}\right) \quad (\text{B3})$$

The factor  $g$  is maximal for  $\theta_r = 90^\circ$ . The total time required to create  $H^{\text{EVO}}$  using the sequence described in Eq. (B2) is  $\tau = 2m\pi/\omega_r$ , where  $m$  is some integer due to the fact that  $H^{\text{EVO}}$  must be created over some integer multiple of rotor periods. In the limit that  $N \rightarrow \infty$ , Eq. (B3) shows that  $g \rightarrow 3/16$  for  $\theta_r = 90^\circ$ .

With the above optimal sequences, the question of how to obtain the maximum dipolar scaling,  $\sigma$ , for a single IS spin pair can now be addressed. Consider the following sequence: the sample first rotates along  $\theta_r = 0^\circ$  for a time  $t$  while the the sequence in Eq. (B1) is applied. The axis of rotation is then changed to  $\theta_r = 90^\circ$  while the sequence in Eq. (B2) is applied (with  $N \rightarrow \infty$ ) for a time  $\tau$ , which is some multiple of a rotor period. From Eq. (22), the anisotropic component of the heteronuclear dipole interaction can be removed when  $t = +4g\tau/3$ . The axis of rotation is then changed to the magic-angle,  $\theta_r = \cos^{-1}(1/\sqrt{3})$ , for application of  $H_{\pm 1}^{\text{DET}}$ . Note that at the magic-angle, high-resolution chemical shift spectra can be obtained, so a possible chemical-shift/heteronuclear coupling correlation experiment can be performed. Using  $g = 3/16$  gives  $\tau = 4t$  and gives a dipolar scaling factor,  $\sigma$ , of

$$\sigma\omega_D = \frac{\omega_D}{t + \tau} \left( \frac{t}{2} (3 \cos^2(\theta) - 1) + 2g\tau \sin^2(\theta) \right) = \frac{\omega_D}{5} \quad (\text{B4})$$

which is the theoretical maximum scaling factor for creating the zero-field Hamiltonian for a heteronuclear spin pair.

The above result is purely hypothetical since the limit  $N \rightarrow \infty$  is not realistic. In addition, for a system of  $I$  spins coupled to a single  $S$  spin, the obtainable scaling factor is reduced due to any homonuclear decoupling method used since some of the experiment has to be performed away from the magic angle. It can be imagined that an extremely large RF is used to decouple the  $I$  spins from each other on a faster time scale than that used to create  $H$ ,  $H^{\text{EVO}}$ , and  $H^{\text{DET}}$ . In this scenario, the scaling factor would be reduced by at least a factor of  $1/\sqrt{3}$ , since that is the largest scaling factor for any pure multiple-pulse decoupling sequence.

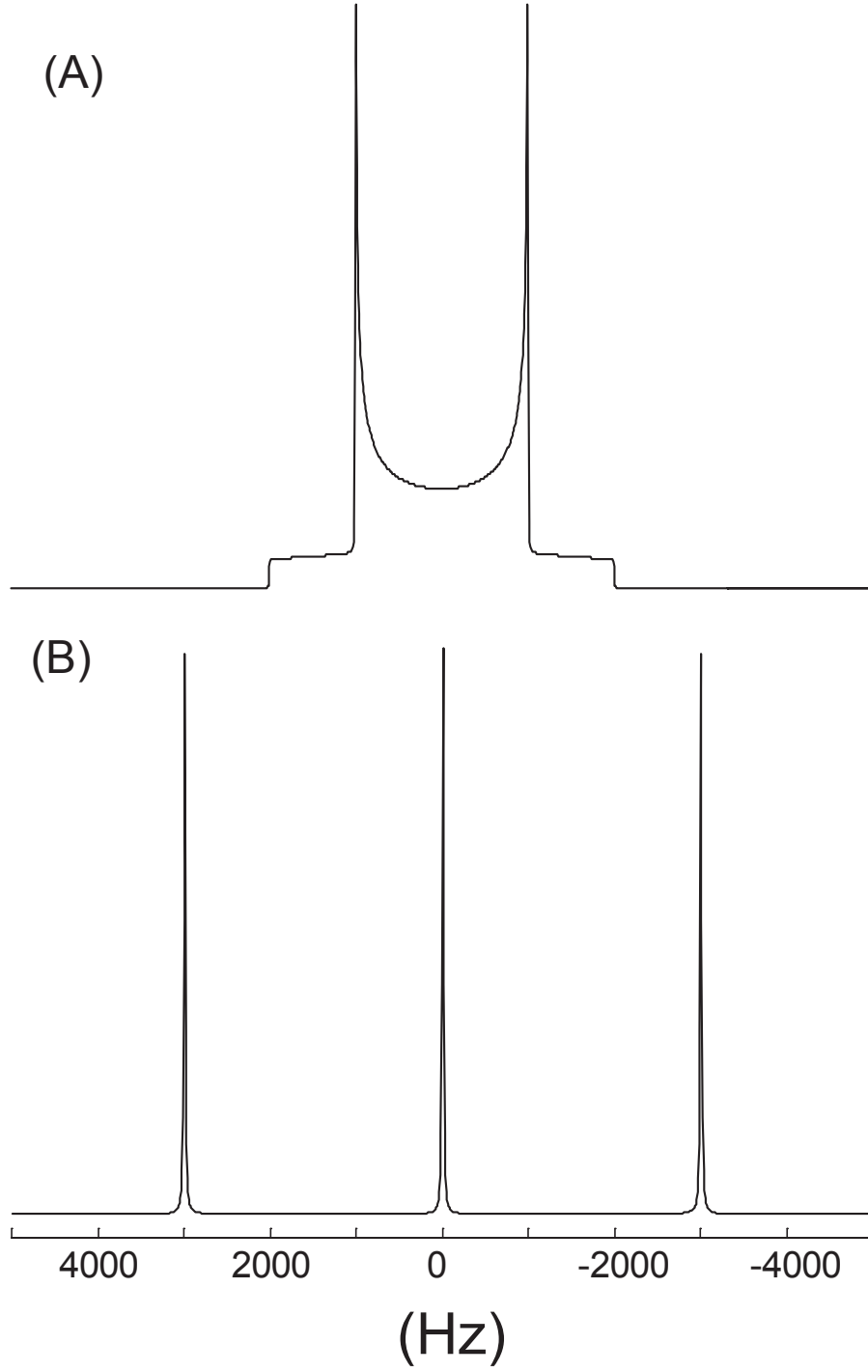


FIG. 1: Simulated spectra for a heteronuclear dipole coupled spin system under (A) high-field and (B) zero-field conditions. A dipolar coupling of  $\omega_D/(2\pi) = 2000$  Hz was used. (A) Pake pattern for a heteronuclear spin system, where the distribution in frequencies is due to the anisotropy of  $H_D^{\text{HF}}$  in Eq. (1). (B) The zero-field consists of three sharp lines at frequencies at 0 Hz and  $\pm 3000$  Hz.

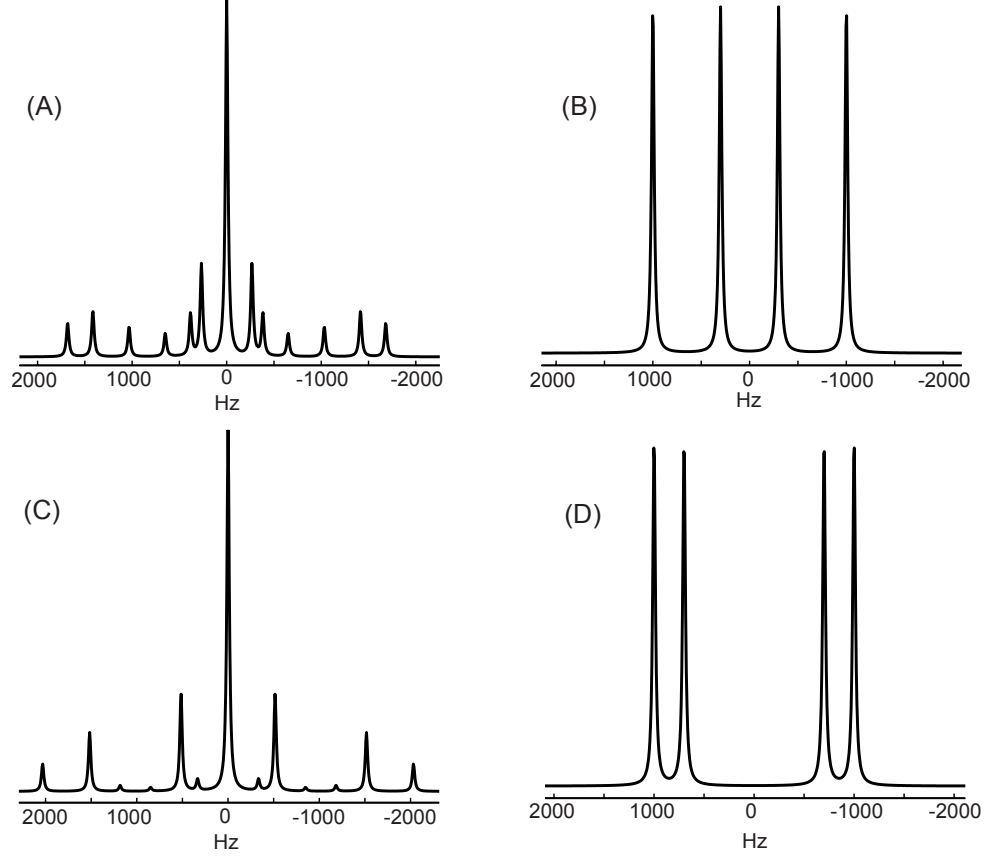


FIG. 2: Comparison of zero-field proton-detected local field spectroscopy with high-field proton-detected local field spectroscopy for two sets of couplings. In (A) and (B),  $\omega_D^{S1}/(2\pi) = 300$  Hz and  $\omega_D^{S1}/(2\pi) = 700$  Hz in (C) and (D).  $\omega_D^{S2}/(2\pi) = 1000$  Hz in all cases. The zero-field Hamiltonian [Eq. (4)] was used in (A) and (C), and the spectra corresponding to the evolution of the total  $I$  magnetization, with intensity in arbitrary units (A.U.). In (B) and (D), a high-field Hamiltonian,  $H = 2\omega_D^{1-2}I_Z^1I_Z^2 + 2\omega_D^{1-3}I_Z^1I_Z^3$ , for a single crystallite orientation ( $\theta_L = 0^\circ$ ) was used to calculate the evolution of transverse magnetization of the  $I$  spins.

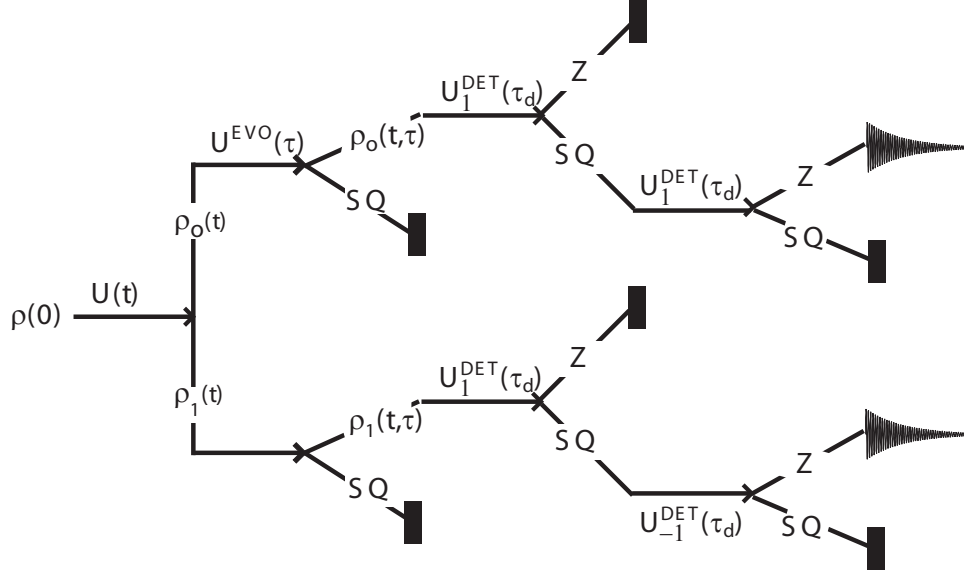


FIG. 3: The basic procedure in order to obtain isotropic proton-detected local field spectra. An initial density matrix,  $\rho(0) = \sum_j a_j I_Z^j$  evolves under  $H$  [Eq. (12)] to give a z-magnetization (Z) term, ( $\rho_0$ ), and single-quantum (SQ) term, ( $\rho_1$ ). Both of these terms then evolve under  $H^{\text{EVO}}$  [Eq. (13)], and only the z-components are kept. Next, evolution occurs from  $\rho_0(t, \tau)$  and  $\rho_1(t, \tau)$  under  $H_1^{\text{DET}}$  [Eq. (14)] into SQ coherence. The SQ coherences are then converted back into z-magnetization for detection, using either  $H_1^{\text{DET}}$  for the pathway originating from  $\rho_0$  or  $H_{-1}^{\text{DET}}$  for the pathway originating from  $\rho_1$ .

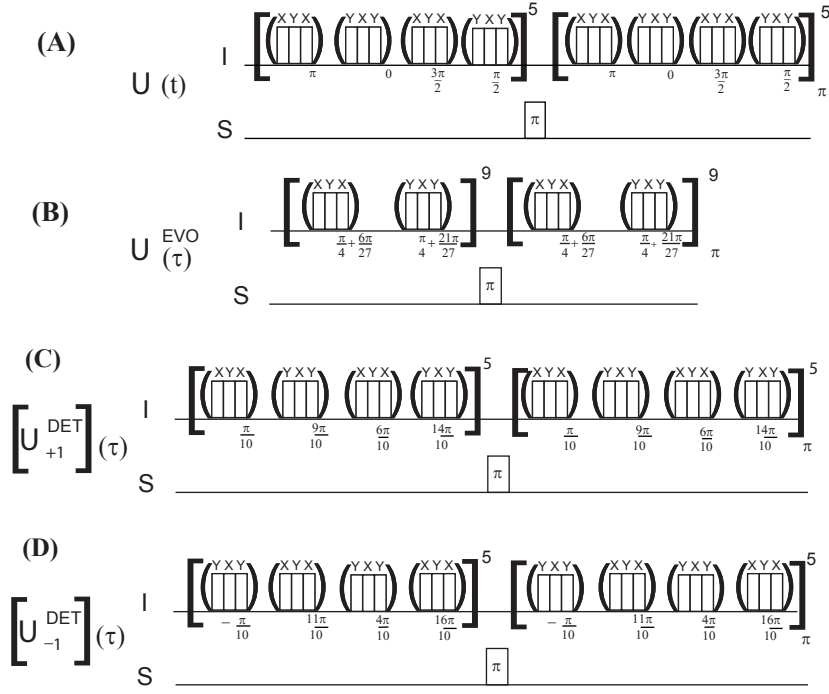


FIG. 4: Basic pulse sequences used to create  $H, H^{EVO}, H_{\pm 1}^{DET}$  needed for HETIE. (A) The pulse sequence which creates  $H$  [Eq. (12)] to lowest order and the corresponding propagator  $U(t)$ .  $\omega_{RF} = (15/2)\omega_r$ , and the total time step for propagator  $U(t)$  is  $t = 8\pi/\omega_r$ . (B) The pulse sequence which creates  $H^{EVO}$  [Eq. (13)] to lowest order and the corresponding propagator,  $U^{EVO}(\tau)$ , with  $\omega_{RF} = (27/4)\omega_r$  and  $\tau = 8\pi/\omega_r$ . (C) and (D) are the pulse sequences and corresponding propagators for  $H_1^{DET}$  and  $H_{-1}^{DET}$  [Eq. (14)] respectively with  $\omega_{RF} = (15/2)\omega_r$ .

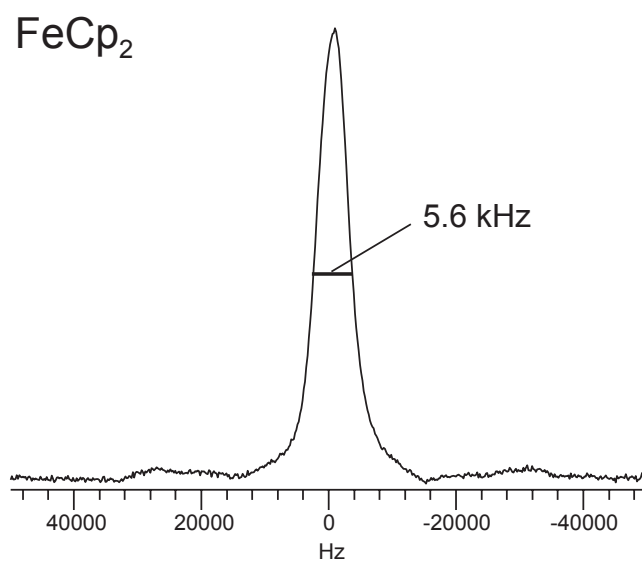
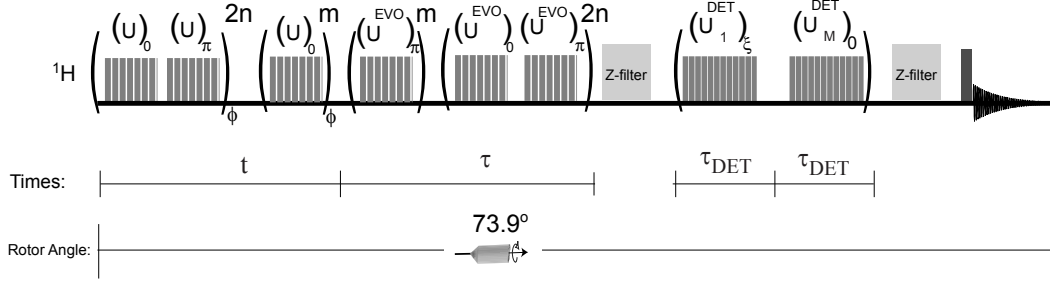


FIG. 5: 300.986 MHz  $^1\text{H}$  NMR spectrum of  $\text{FeCp}_2$  spinning 15 kHz at  $\theta_r = 73.9^\circ$



experiment	$\phi$ (deg)	$\xi$ (deg)	M	receiver phase
X <sub>1</sub>	0	0	1	-1
X <sub>2</sub>	0	180	1	1
Y <sub>1</sub>	180	0	1	-1
Y <sub>2</sub>	180	180	1	1
2 * X <sub>3</sub>	0	0	-1	1
2 * X <sub>4</sub>	0	180	-1	-1
2 * Y <sub>3</sub>	180	0	-1	-1
2 * Y <sub>4</sub>	180	180	-1	1

FIG. 6: Actual experiments performed for the demonstration of HETIE methodology to obtain isotropic proton-detected local-field spectra. The pulse sequence, along with the corresponding phase cycle, is presented. Definitions of  $U$ ,  $U^{\text{EVO}}$ , and  $U_{\pm 1}^{\text{DET}}$  are given in Fig. 4, which include the series of  $180^\circ$  pulses which are not explicitly shown in this figure. The points in  $t_1$  are parameterized by  $2n + m$ ,  $n = \{0, 1, 2, \dots\}$  and  $m = 1$  for odd numbered points and  $m = 0$  for even numbered points. For the above experiment,  $t = \tau = (2n + m) * 16\pi / \omega_r$ . The first four experiments correspond to evolution along  $\rho_0$  in Fig. 3. The last four experiments correspond to evolution along  $\rho_1$  in Fig. 3. The last four experiments have to be performed twice as required from Eq. (25).

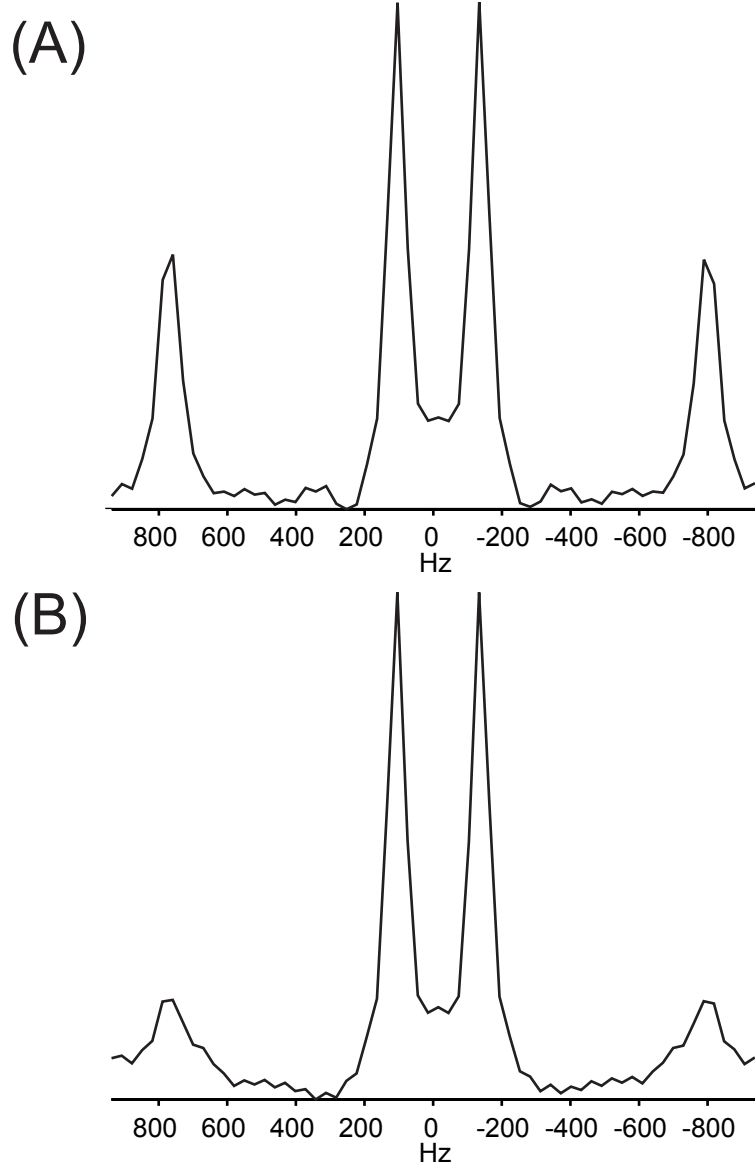


FIG. 7: Simulation of the performance of the HETIE pulse sequence (Figure 6) using the SIMPSON program<sup>31</sup>. The heteronuclear dipolar couplings of  $\omega_D^{12}/(2\pi) = 13.425$  kHz and  $\omega_D^{13}/(2\pi) = 1.458$  kHz were used in both simulations, and a homonuclear dipolar coupling of  $\omega_D^{23}/(2\pi) = 1$  kHz was used. (A) Ideal  $\text{CH}_2$  spin system in the absence of CSA. (B) non-ideal spin system with the CSA of 5 kHz for each proton.

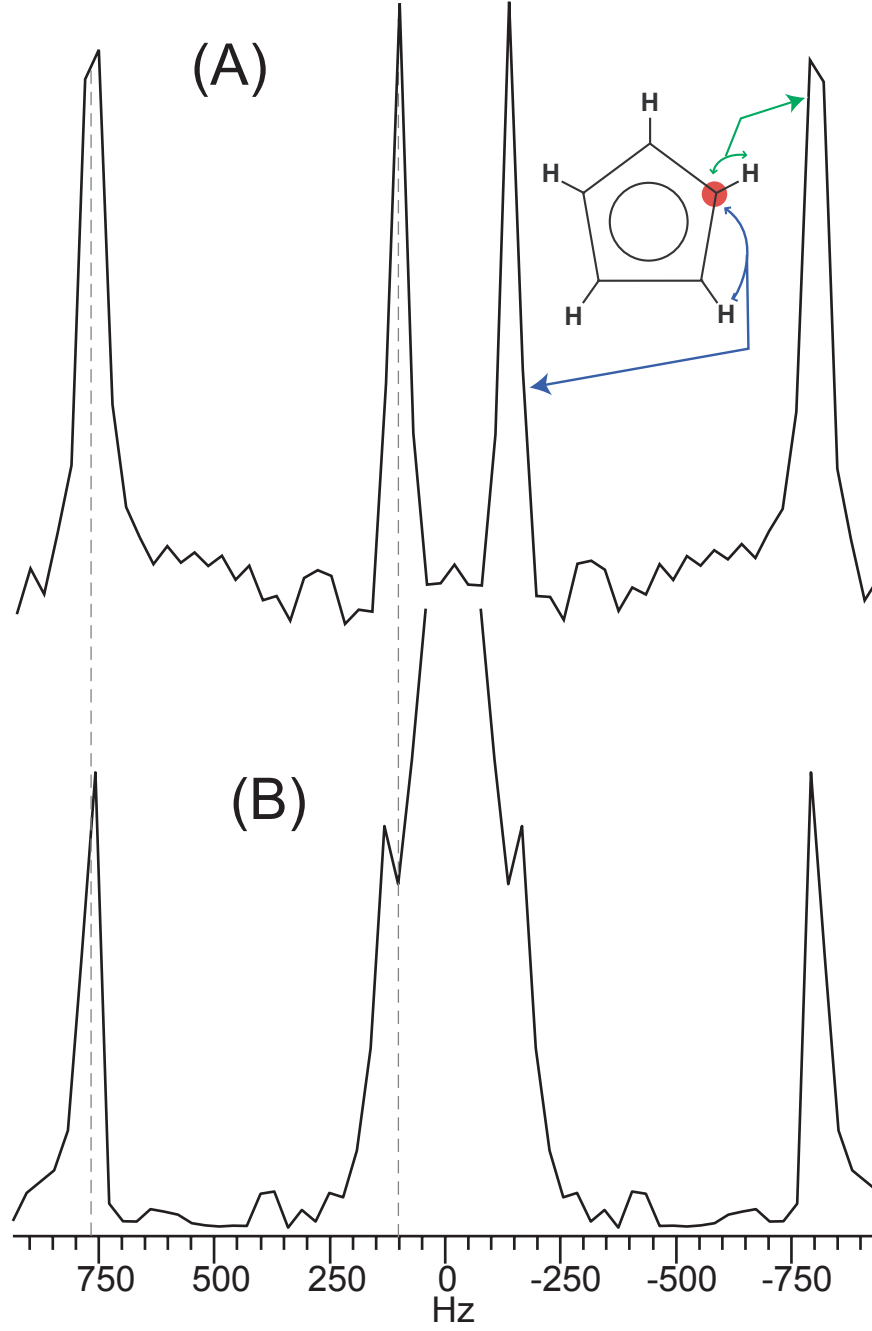


FIG. 8: HETIE experiment and simulation comparison for FeCp<sub>2</sub>. (A) The simulation uses the couplings as determined from diffraction studies<sup>22</sup>. (B) The experimental power spectrum was acquired at 300MHz.  $\theta_r = 73.9^\circ$  and  $\omega_r/(2\pi) = 15$  kHz.

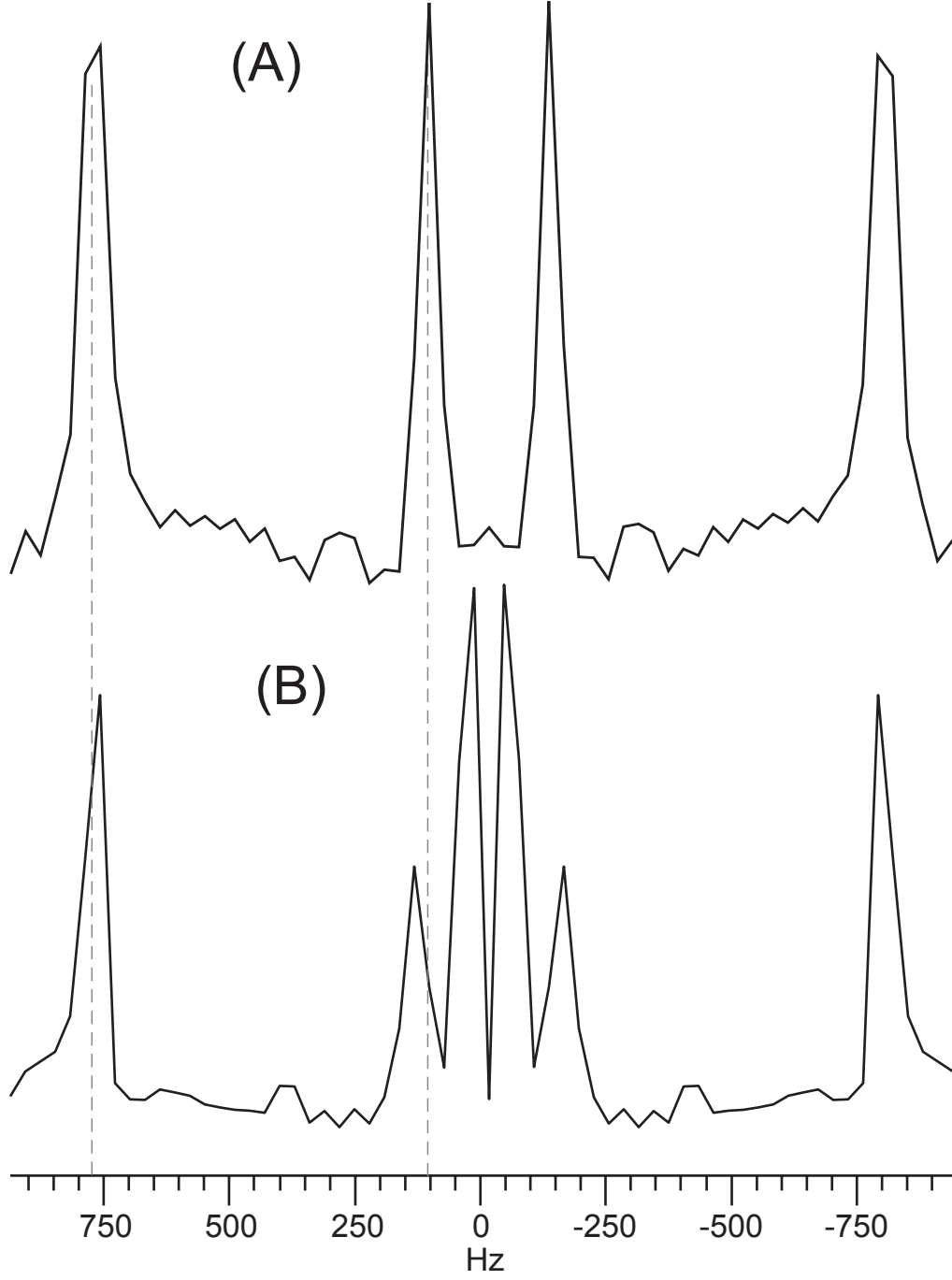


FIG. 9: HETIE experiment and simulation comparison for  $\text{FeCp}_2$ . (A) The simulation is the same as in Figure 8. (B) The *deconvolved* experimental power spectrum was acquired at 300MHz.  $\theta_r = 73.9^\circ$  and  $\omega_r/(2\pi) = 15$  kHz.

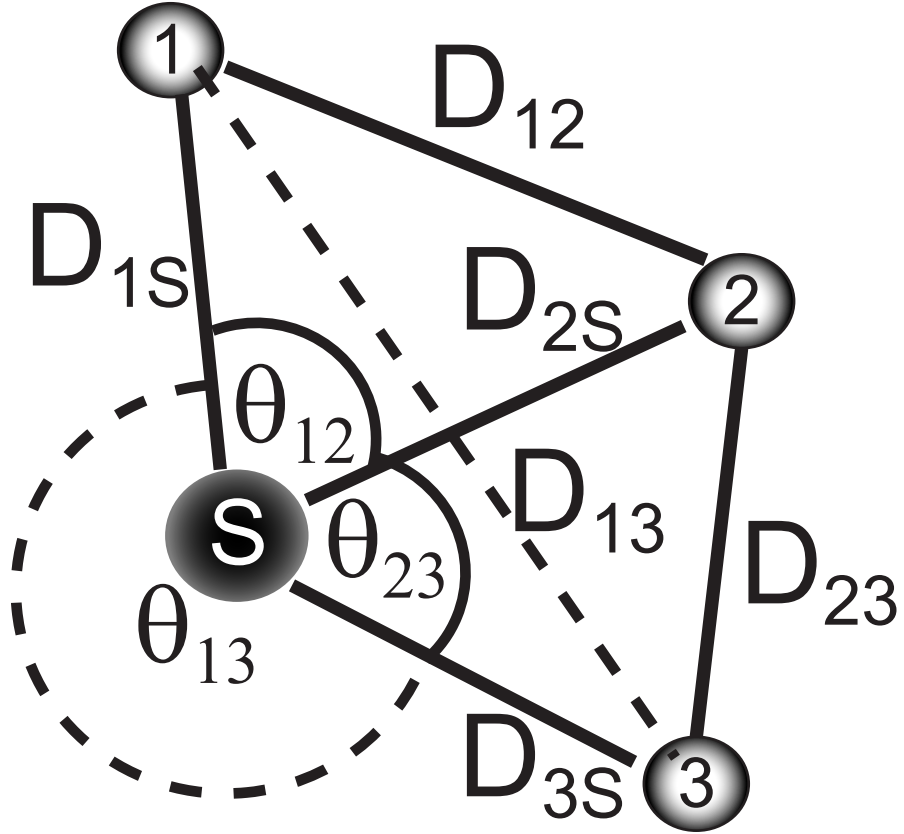


FIG. 10: An  $I_3S$  system. HETIE, in principle, can determine  $D_{1S}$ ,  $D_{2S}$ , and  $D_{3S}$ . In order to fully determine the structure, either the relative angles ( $\theta_{12}$ ,  $\theta_{13}$ , and  $\theta_{23}$ ) or the homonuclear distances ( $D_{12}$ ,  $D_{13}$ , and  $D_{23}$ ) need to be determined.